land

Article

Performance Evaluation for the Expansion of Multi-Level Rail Transit Network in Xi'an Metropolitan Area: Empirical Analysis on Accessibility and Resilience

Yulin Zhao [1], Linkun Li [1], Zhishuo Zhang [1] and Daniel (Jian) Sun [1,2,*]

[1] School of Future Transportation, Chang'an University, Xi'an 710064, China; 2020900014@chd.edu.cn (Y.Z.); 2021901888@chd.edu.cn (L.L.); 2021903439@chd.edu.cn (Z.Z.)
[2] Institute of National Security, Shanghai Jiao Tong University, Shanghai 200240, China
* Correspondence: jiansun@chd.edu.cn

Abstract: As the main form of new urbanization, the coordinated development of cities in metropolitan areas requires reliable and efficient rail transit skeleton support. However, in the rapid development of metropolitan areas, the layout and analysis of multi-level rail transit systems have a certain lag. Taking the Xi'an metropolitan area as an example, this study analyzes the comprehensive accessibility and resilience of the multi-level rail transit network, and proposes an expansion plan accordingly. The traffic analysis zone (TAZ) is divided by towns and streets, and the relationship between points of interest (POIs) and the regional average level is analyzed using DEA. The improved weighted average travel time model is built with the analysis results as regional weights; a site selection model based on multiple construction influencing factors is proposed, and four expansion plans, namely, economic optimal, environmental optimal, transport optimal, and integrated optimal, are designed. The peak passenger flow scenario and the "failure–reparation" scenario during the entire operation period are designed to analyze the resilience of four plans, and the resilience is quantified by the elasticity curve of the maximum connected subgraph ratio (MCSR) changing over time. The research results show that the transport optimal plan has the best comprehensive accessibility and resilience, reducing travel costs in Houzhenzi Town, which has the worst accessibility, by 34%. The expansion model and evaluation method in this study can provide an empirical example for the development of other metropolitan areas and provide a reasonable benchmark and guidance for the development of multi-level rail transit networks in future urban areas.

Keywords: metropolitan area; rail transit; site selection; integrated transportation network accessibility; resilience; Geographical Information Systems (GIS); data envelopment analysis (DEA)

Citation: Zhao, Y.; Li, L.; Zhang, Z.; Sun, D. Performance Evaluation for the Expansion of Multi-Level Rail Transit Network in Xi'an Metropolitan Area: Empirical Analysis on Accessibility and Resilience. *Land* **2024**, *13*, 1682. https://doi.org/10.3390/land13101682

Academic Editor: Thomas W. Sanchez

Received: 23 August 2024
Revised: 7 October 2024
Accepted: 12 October 2024
Published: 15 October 2024

1. Introduction

Metropolitan is an important urbanized spatial form with a megacity or a large city with strong radiation as the center and a 1 h commuting circle as the core range. Public transportation, especially rail transportation, has a significant impact on promoting the coordinated development of cities within the metropolitan area. According to the CEIC database statistics (https://www.ceicdata.com.cn/zh-hans/china/public-transit-summary: accessed on 20 September 2024) [1], China's rail transportation passenger volume has experienced an upward trend, gradually increasing from 8.7 million in 2012 to 29.4 million in 2023. The rail transit system has become the main transportation framework for promoting urban development and enhancing regional competitiveness [2].

During the last 5–10 years, metropolitan areas in China have been experiencing rapid development, along which the passenger flow and mileage of rail transit have increasingly become unbalanced during the process. This, to some extent, induces the major gaps in the connection and layout between rail transit at all levels. Although Xi'an has achieved an extraordinary domestic and international reputation, the metropolitan area was established relatively late, and the transportation connection between the metropolitan core area and other groups is still weak [3]. Therefore, to enhance the comprehensive competitiveness of the metropolitan area, promoting the development of a multi-level rail transit network has become the primary task of the metropolitan area [4].

This paper proposes a rail transit network expansion plan by incorporating various construction factors, together with a plan evaluation method based on the two levels of comprehensive transportation network accessibility and rail transit network resilience. Specifically, the weighted average travel time model was first improved by the data envelopment analysis (DEA) model and point of interest (POI) data [5,6], and the accessibility of the current comprehensive transportation network of the Xi'an metropolitan area was evaluated and analyzed. Then, a site selection model based on multiple construction influencing factors was constructed, and four rail transit expansion plans were proposed. In order to obtain the optimal expansion plan, the improved weighted average travel time model was introduced to evaluate the comprehensive transportation accessibility, and two network random attack scenarios were constructed to evaluate the resilience of the multi-level rail transit network. The results demonstrate that the optimal transportation expansion plan has the highest network resilience while significantly improving the accessibility of the study area.

Rail transit line expansion and station site selection have been widely investigated. Bussieck et al. [7] analyzed the rail transit network planning model and solution method based on the train timetable. Targeting travel time reduction and service quality improvement, Li et al. [8] proposed a rail transit network expansion model based on a mixed integer programming model. Ghorbanzadeh et al. [9] used the multi-index analytic hierarchy process and combined it with ArcGIS to analyze the metro station site selection scheme in developing countries. Cai et al. [10] proposed a metro station site selection method based on LeaderRank and Gaussian mixture model (GMM) to establish a metro-passenger traffic zoning weighted network and station location prediction model, and combine taxi GPS trajectories to plan the location of new metro stations. Previous studies mainly focused on rail transit line expansion and station location selection using passenger OD data, and seldom considered various factors affecting construction.

With the acceleration of urbanization, studies on public transportation systems have become increasingly popular, including hybrid optimization of bus–rail systems [11,12], bus–subway transfer efficiency based on Smart Card Data [13], and TOD efficiency research [14]. As a public transportation system with a wider service scope, rail transit systems have received more attention in metropolitan area research. The enhancement of multi-level rail transit networks aims to optimize travel within metropolitan areas, with accessibility frequently serving as a key evaluation metric. Such networks comprise four primary components: high-speed rail, intercity rail, urban rail, and metro. In contrast to single-level rail systems, multi-level networks present a broader impact area and potential losses in the event of an accident. Consequently, the resilience of the entire system is also a critical factor in assessing the relative benefits and drawbacks of a multi-level rail transit network.

Accessibility is defined as the degree of interaction between nodes within the network, which was originally used to determine the intensity of spatial interaction [15] and is now widely used in urban development analysis [16]. Liu et al. [17] and Zhou and Yang [18] analyzed the accessibility of metro system from the perspective of network expansion, which, however, ignored integrated travel modes and cost. Li et al. [19] captured the differences in health service accessibility at the spatiotemporal level through the Gini coefficient and Theil index, and introduced the bivariate local Moran's I to evaluate the relationship between population density and health service accessibility. Lucas et al. [20] introduced the payroll to analyze the relationship between income and accessibility; Sun [21] introduced urban congestion duration into the weighted average travel time model, and combined it with tourism economy to analyze the changes in transportation accessibility and the intensity of tourism economic connections between cities before and after the opening of the Daxi High-speed Railway. Yu and Cui [22] divided travelers according to income and discussed the impact of urban rail transit based on accessibility and fairness. Compared with the regular accessibility analysis based solely on time, the integrated cost enriches the impedance type and is more consistent with the actual situation, although the analysis of travel purposes may be ignored.

For resilience research of rail transit systems, previous studies have analyzed the robustness and full disturbance cycle of rail transit networks. Regarding robustness, most studies have adopted the coupled map lattice (CML) model to simulate cascading failures in large passenger flow [23,24] or disaster scenarios [25], and to quantify robustness based on network structure indicators or the degree of passenger flow decline. Xu et al. [26] proposed a multi-modal public transit networks (MPTNs) for robustness analysis to avoid the shortcomings of one single mode. Regarding the full disturbance cycle analysis, Wen et al. [27] proposed a maximum survivability–minimum recovery time approach to analyze the survivability and recoverability of the urban rail transit–bus network before and after the disturbance. Sun and Guan [28] measured the metro network vulnerability by investigating the disruption from the line operation perspective. Yin et al. [29] proposed a hybrid method based on knowledge and data to analyze the quantitative relationship between rail transit network resilience and accident types.

2. Integrated Accessibility Assessment Method for Metropolitan Areas

2.1. Weighted Average Travel Time Model Based on POIs

In the traditional weighted average travel time model, the geometric mean of regional GDP and population size is used as the regional weight M_j to reflect the influence of regional size on residents' willingness to move [30]. On this basis, this study introduces the impact of POIs on travel intention, considering three travel purposes: commuting, shopping, and traveling, and introducing the influence of residential places and transportation facilities. Five POI types, companies, attractions, malls, residence facilities, and transportation facilities, are used to evaluate the attractiveness of regional travel. Referring to the definition of regional weights in the traditional weighted average travel time model, the effect of regional vitality on residents' willingness to move is evaluated by the benefits between the number of POIs and the regional GDP and population. This indicator is calculated by the input-oriented CCR model in data envelopment analysis (DEA) [31], which evaluates the relative benefits between decision-making units (DMUs). Two commonly used models [32] are the CCR model assuming constant returns to scale and the BCC model assuming variable returns to scale. The township and street districts are used as TAZs [33] and decision-making units (DMUs), and the center of TAZs serves as the OD point for travel analysis. A 3 km buffer is set, and the number of five types of POIs within the buffer are counted. The min–max normalization method [34] is used to eliminate the differences in the total amount of different types of POIs. The standardized data are used as the input variable, and the average level E_j of each region is used as the output variable. The regional average level is calculated based on GDP, population size, and regional area. The area factor is introduced into the regional weight of the original weighted average travel time model to eliminate the differences based on administrative divisions. The calculation formula is as follows:

$$E_j = \sqrt{\left(P_j * G_j\right) \Big/ S_j} \tag{1}$$

where P_j is the population of area j, in 10^4 persons; G_j is the GDP of area j, in 10^4 RMB; S_j is the area of region j in km^2.

Since regional GDP, population size, and regional area are all fixed values, the CCR model with constant returns to scale is used to analyze the impact of regional vitality on people's willingness to move. The relevant model is as follows [35]:

$$\theta^{i^*} = Min\theta^i - \varepsilon\left(\sum_m^M s_m^- + \sum_n^N s_n^+\right) \tag{2}$$

Subject to the following:

$$\theta^i x_m^i = \sum_{j=1}^J x_m^j \lambda^j + s_m^- \tag{3}$$

$$y_n^i = \sum_{j=1}^J y_n^j \lambda^j - s_n^+ \tag{4}$$

$$\sum_{j=1}^J \lambda^j = 1 \tag{5}$$

$$\lambda^j \geq 0 \tag{6}$$

$$s_m^- \geq 0 \tag{7}$$

$$s_n^+ \geq 0 \tag{8}$$

where θ^{i^*} is the relative magnitude of the impact of the regional vitality on people's willingness to move; y_n^j is the output number of each variable n of region j; x_m^j is the input number of each variable m of region j; j is the number of regions ($j = 1, \ldots, 330$); n is the output variable, $n = 1$, E_j indicating the regional average level; m is the input variable ($m = 1, \ldots, 5$; $m = 1$: the number of standardized companies, $m = 2$: the number of standardized attractions, $m = 3$: the number of standardized malls, $m = 4$: the number of standardized residence facilities, $m = 5$: the number of standardized transportation facilities; λ^j is the weight of each region; s_m^-, s_n^+ are the slack for input variable and output variable, respectively.

The relative benefits of each region obtained by the CCR model are used as regional weights to improve the weighted average travel time model. The relevant formula is as follows:

$$A_i = \frac{\sum_{j=1}^n (T_{ij} * M_j)}{\sum_{j=1}^n M_j} \tag{9}$$

where A_i is the weighted average travel time of area i based on POIs, that is, travel cost, which is used to reflect the accessibility of the area. The larger A_i indicates lower accessibility; T_{ij} is the shortest travel time distance from area i to area j; M_j is the relative benefit θ^{i^*} of each region obtained by the CCR model.

2.2. Initial State integrated Traffic Accessibility Analysis

2.2.1. Data Processing

According to the "Xi'an Metropolitan Area Development Plan" [36], the towns and streets in the metropolitan area are taken as analysis zones, and the weighted cost distance instead of the actual distance is used to analyze the accessibility of each traffic zone. Figure 1a presents the administrative regions for the research area, and the traffic zones divided by towns and streets are shown in Figure 1b.

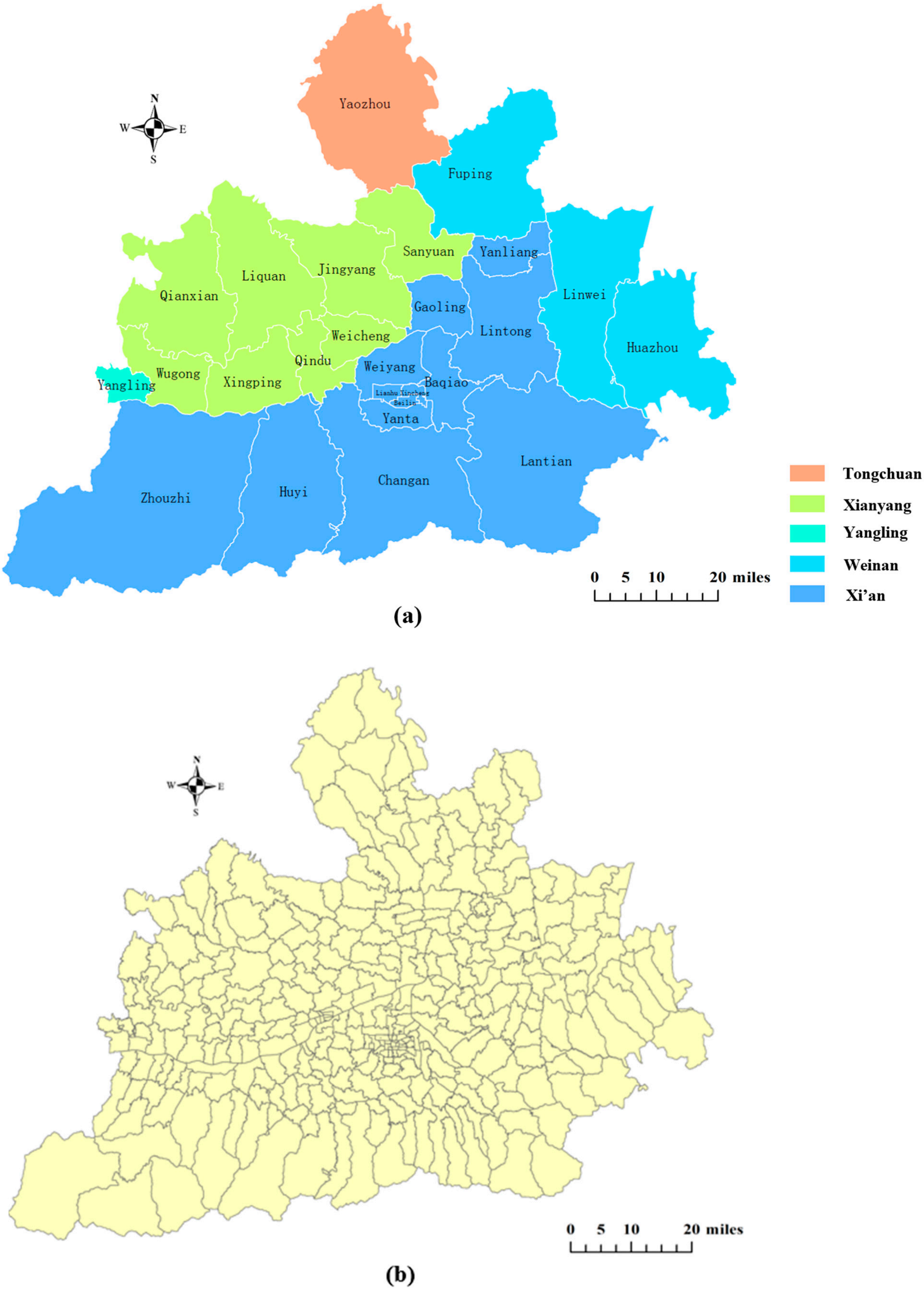

Figure 1. (**a**) Schematic diagram of the study area. (**b**) Schematic diagram of TAZ division.

Transportation and geographic data were acquired as follows. The base map and road network for the study area were obtained from OpenStreetMap (https://openmaptiles.org/: accessed on 23 November 2023) [37], while railway and station data for high-speed rail, intercity rail, urban rail, and metro were obtained from AutoNavi Map (https://lbs.amap.com/: accessed on 25 November 2023) [38]. The metro data include both planned and operational lines as of July 2023, with some intercity railways and urban rails based on the planning documents from The China Railway First Survey and Design Institute Group Co., Ltd. (http://www.fsdi.com.cn/: accessed on 25 November 2023) [39].

Population and economic data were derived from the 2020 seventh national census (https://www.stats.gov.cn/sj/pcsj/rkpc/7rp/zk/indexch.htm: accessed on 26 November 2023) [40], encompassing GDP and population figures for each town and street within the study area. Additionally, the POI data, totaling 14 categories and 164 types, were collected using the AutoNavi Map open platform.

Highway network data are categorized into six levels with the assigned speed limits: expressway at 100 km/h; urban expressway at 80 km/h; urban trunk road at 60 km/h; urban secondary road at 40 km/h; urban branches and rural roads at 30 km/h and 20 km/h, respectively. Rail transit data are segmented into two groups: metro data with a speed set to 35 km/h; high-speed rail, intercity, and urban rail data adjusted based on their operational characteristics.

Assumptions:

- Travelers transferring between highway and rail transit have to walk, with an average speed of 1.2 m/s; the transfers between high-speed rail, intercity and urban rail, and metro are also set to walking, with a speed of 1.2 m/s; the transfer time between the three rail transit modes of high-speed rail, intercity rail, and urban rail is set to 8 min.
- Transfers between metro lines are set to be within the station, with the transfer time as 4 min.

2.2.2. Accessibility of Integrated Transportation Network in Xi'an Metropolitan Area

A 3 km radius buffer zone centered on the TAZ centroid was established to obtain the number of five types of POIs within each TAZ's buffer zone. The results are shown in Figure 2.

Due to the differences in the total amount and categories of various POIs, the min–max normalization method is used to eliminate POI differences. Then, the CCR model is constructed and analyzed in combination with the GDP, population size data, and area of TAZ. Figure 3 shows the distribution of regional attractiveness estimated by the model. The average attractiveness score of 330 regions is estimated to be 0.306. The minimum, maximum, and standard deviation are estimated to be 0.003, 1.00, and 0.222, respectively. This distribution feature reflects the extremely unbalanced distribution of travel attractiveness of various towns and streets in the Xi'an metropolitan area.

In ArcGIS, an integrated transportation network was constructed by using travel time as impedance for OD cost matrix analysis in order to calculate the average travel time cost for each zone. Subsequently, the weighted average travel time (A_i) was computed for each transportation community based on factors including GDP, population, and POI correction coefficients. Since the TAZ center is used as the OD point for analysis in this paper, the calculated accessibility index is only located at these points, and other areas are not assigned values. Therefore, in order to more clearly observe the comprehensive accessibility results of the entire Xi'an metropolitan area, this paper divides the study area into 100 $\times$ 100 m grid data, uses Kriging interpolation [41] to obtain the comprehensive travel cost of each grid, and visualizes the result, as shown in Figure 4:

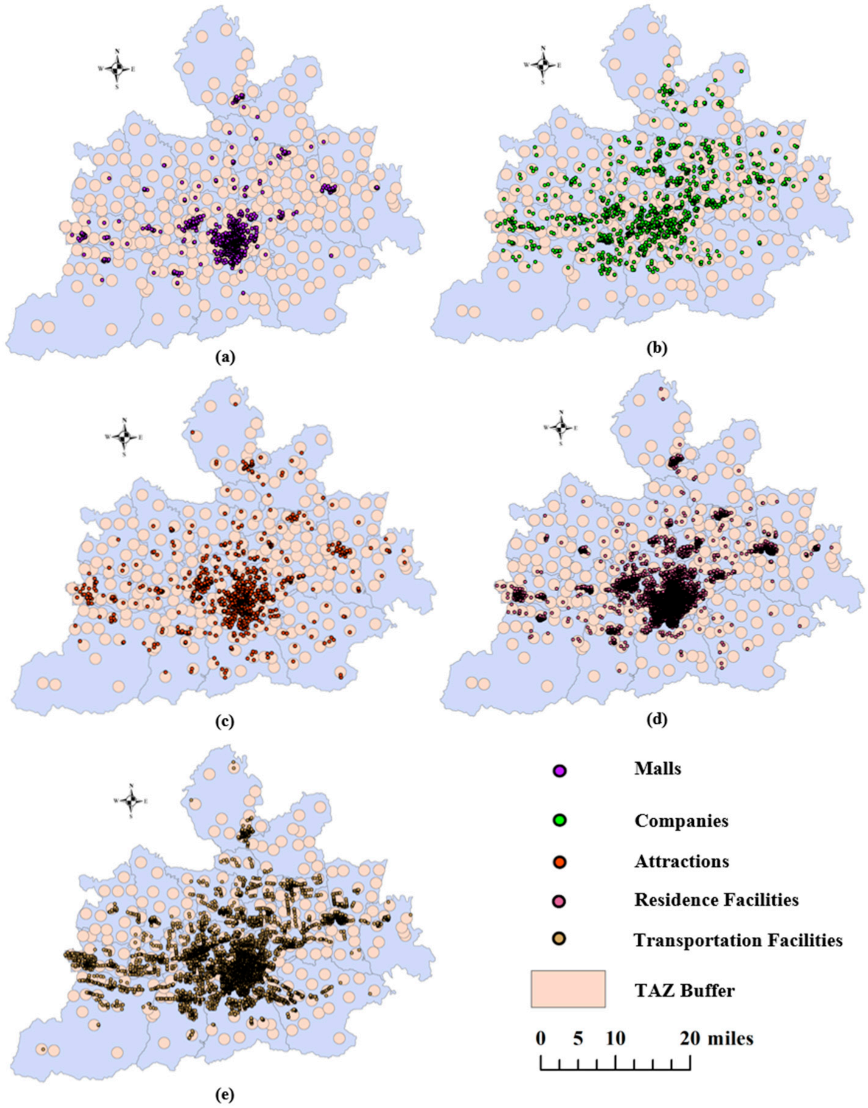

Figure 2. Overlapping results of TAZ buffer and three POIs; (**a**–**e**) represent the quantity of malls, companies, attractions, residence facilities, and transportation facilities within TAZ, respectively.

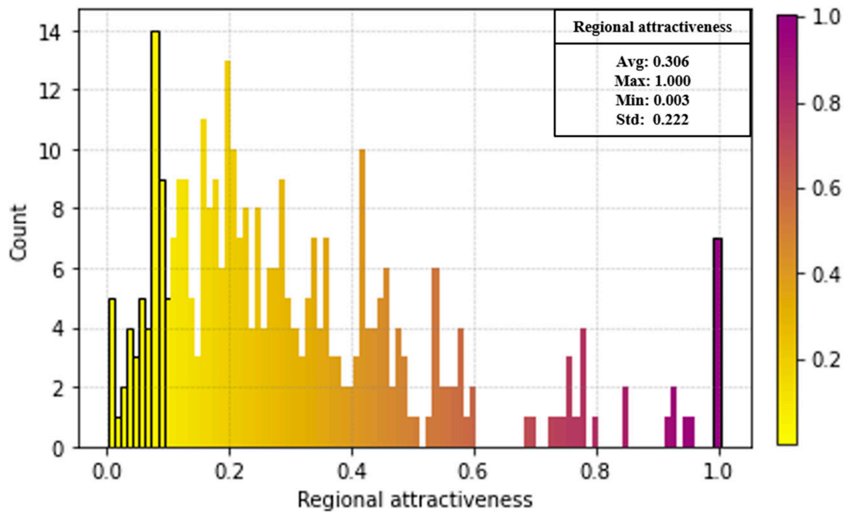

Figure 3. Distribution of regional attractiveness.

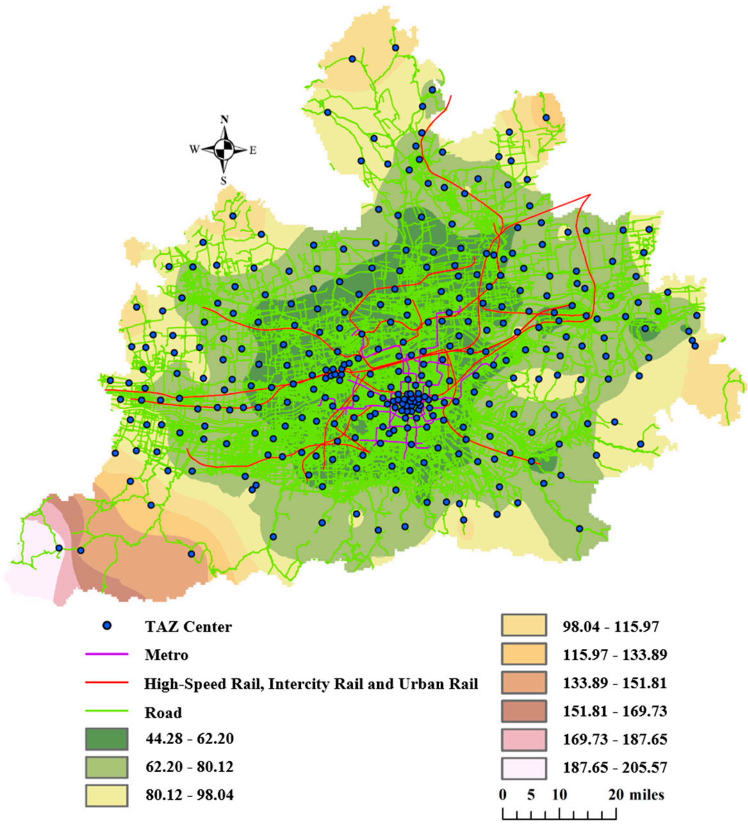

Figure 4. Weighted average travel time based on POIs.

3. Rail Transit Network Expansion Plan and Accessibility Assessment

3.1. Expansion Plans Based on Multiple Construction Influencing Factors

3.1.1. Site Selection Model and Solution

To enhance accessibility and reduce integrated travel costs in the Xi'an metropolitan area, a rail transit expansion plan based on multiple construction influencing factors was proposed. Initially, the POI heat value overlay analysis was conducted to identify preliminary expansion site selections. Six types of transportation-related POIs were considered: malls, companies, transportation facilities, educational places, attractions, and residence facilities. The Klee method was used to quantify the influence of the six types of POIs, which is an integrated evaluation method to quantify subjective judgments. The basic steps of the Klee method are as follows [42,43]:

Assuming that there are n evaluation indicators i, corresponding to m evaluation subjects, R_j represents the importance of the comparison between the evaluation items, K_j represents the evaluation value. The last evaluation subject does not have a pairwise comparison counterpart, so R_m does not exist, and K_m is set to 1. The evaluation value K_j is calculated as Equation (10):

$$K_{j-1} = R_{j-1} * K_j \tag{10}$$

where $j = n, n-1, \ldots, 1$.

Using w_i to represent the normalized weight of the i-th item, the calculation is shown in Equation (11):

$$w_i = \frac{K_i}{\sum_{j=1}^{n} K_j} \tag{11}$$

Table 1 presents the association matrix quantifying the weights of the six types of POIs as described.

Table 1. Correlation matrix of six types of POIs.

Type of POI	Importance Coefficient R_j	Evaluation Value K_j	Weights W_j
Malls	3	5	0.242
Companies	1/3	5/3	0.081
Transportation Facilities	5	5	0.242
Educational Places	1/7	1	0.048
Attractions	7	7	0.339
Residence Facilities	—	1	0.048
Overall	—	20.667	1.0

Kernel density analysis in ArcGIS was employed to assess the POI heat values. Initially, the vector base map of the Xi'an metropolitan area was gridded into 100 m × 100 m cells, and heat values for six POI types were initialized according to Equation (12):

$$E = W * f \tag{12}$$

where E is the initial value of the POI center heat, W is the corresponding weight, and f is the initial series, selected as 1000 here.

Figure 5a–f present the results of the kernel density analysis for the six types of POI, respectively.

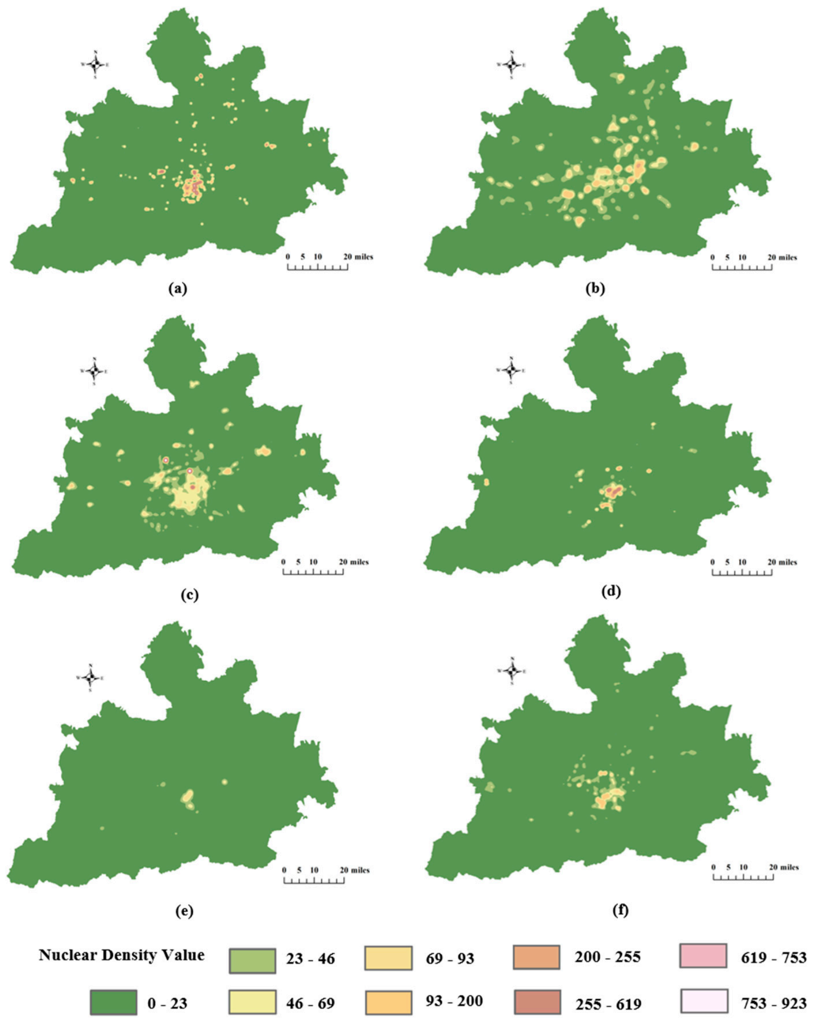

Figure 5. Kernel density analysis results of six types of POI; (**a**–**f**) represent malls, companies, transportation facilities, educational places, attractions, and residence facilities, respectively.

Overlay analysis, weighted by POI types in the association matrix, was carried out with a 100 m × 100 m grid aligned with the base map. Figure 6a displays the resulting POI combined heat values. Figure 6b presents the visualization of the values and sites after incorporating metro, high-speed railways, intercity railways, and urban railways.

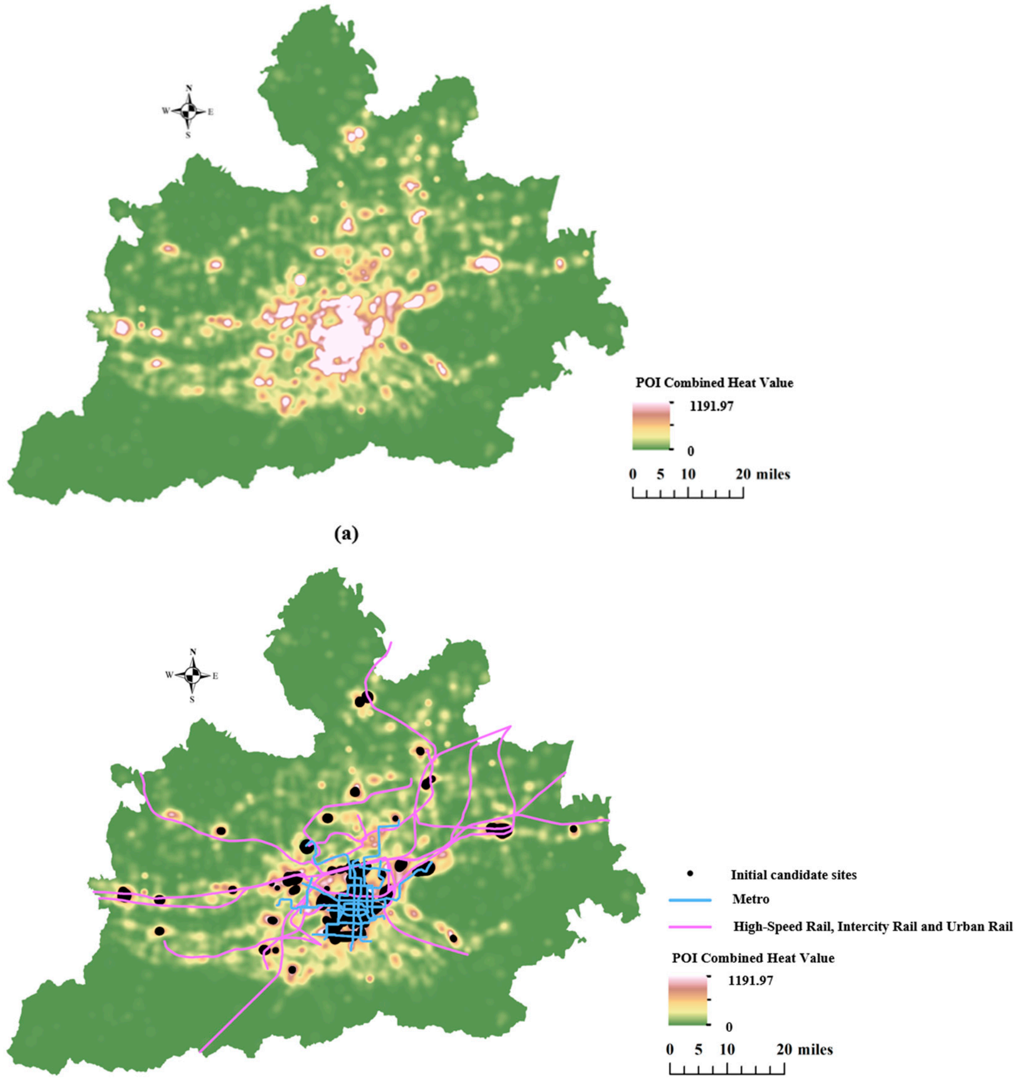

(b)

Figure 6. POI combined heat value and preliminary candidate sites. (**a**) Visualization of Kriging interpolation of POI combined heat value, and (**b**) visualization of adding preliminary candidate sites and rail transit lines.

Based on Figure 6b, the initial candidate sites align closely with the rail transit line, confirming the feasibility of the method. Initially, 38,069 candidate sites were identified based on POI heat values, which was deemed excessive. To refine selection, land use data were introduced, revealing that the planned sites exclusively align with highway networks without intersecting with other land types. Candidate sites were then intersected with land use data, reducing the number to 2286.

These sites underwent evaluation across economic budget, environmental impact, and transport connection aspects using Equations (13)–(15):

$$F_i^1 = \sum \left(s_i * p_i * \alpha_i\right) \tag{13}$$

$$F_i^2 = Greenland(i) + Water(i) \tag{14}$$

$$F_i^3 = Bus(i) + Con(i) \tag{15}$$

where F_i^1 is a negative influencing factor, representing the impact of the economic budget; s_i is the area of land acquisition and demolition of different types, in m^2; p_i is the land market price; α_i is the land compensation coefficient, as 1.2; F_i^2 is a negative influencing factor, representing the environmental impact; F_i^3 is a positive influencing factor, representing the impact on transport.

The parameters of relevant indicators are obtained as follows:

Economic budget parameters: Count land areas (commercial, residential, industrial, public) within a 500 m radius buffer zone around each alternative station, calculating the indicator based on Equation (13).

Environmental impact parameters: With the candidate site as the center and a 500 m radius as the buffer zone, which intersects with the green space and water area, respectively, obtain the green space area and river area within the influence range of each candidate site.

Transport connection parameters: Assess the connection between the alternative station and bus stations/networks. Initially, count alternative stations within a 300 m radius of the bus station, then compute the transport connection index based on the counts and the number of bus lines serving the bus station.

These indicators are counted individually and standardized using SPSS. The integrated indicator F is derived from the standardized indicators by Equation (16):

$$F_i = w_3 F_i^3 - w_1 F_i^1 - w_2 F_i^2 \tag{16}$$

where F_i is the integrated index of the factors affecting construction for the i-th alternative site; w_1, w_2, and w_3 are the corresponding weights of the three indicators; $w_1 + w_2 + w_3 = 1$.

To describe different factor preference, four expansion plans are set: economic optimal, environment optimal, transport optimal, and integrated optimal. The specific weight settings of different plans are as below:

- Economic optimal expansion plan ($w_1 = 1,\ w_2 = 0,\ w_3 = 0$): Aims at the cost of land acquisition, assigning a weight of 1 to economic budget, and other factors are weighted at 0.
- Environment optimal expansion plan ($w_1 = 0, w_2 = 1, w_3 = 0$): Aims to minimize the impact of construction on the environment, emphasizing environmental protection. Thus, environmental impact is weighted at 1 and other factors weighted at 0.
- Transport optimal expansion plan ($w_1 = 1, w_2 = 0, w_3 = 1$): Aims to integrate rail transit and bus systems, with transport connection weighted at 1, and other factors weighted at 0.
- Integrated expansion plan ($w_1 = 1/3, w_2 = 1/3, w_3 = 1/3$): Aims to balance economic budget, environmental impact, and transport connectivity; each factor is weighted equally at 1/3.

The candidate sites set M = $\{m_1, m_2, \ldots m_i, \ldots m_j, \ldots m_n\}$, i, j = 1, 2, …, n, m_i is the i-th candidate site, m_i^x and m_i^y are the latitude and longitude of candidate site i, respectively; suppose the existing site set S = $\{s_1, s_2, \ldots s_k, \ldots s_p\}$, k = 1, 2, …, p, s_k is the k-th candidate site, and s_k^x and s_k^y are the latitude and longitude of existing site k, respectively. Using a 0–1 decision variable X_i to indicate whether site i in the candidate site set M is selected, 0 indicates a nonexpansion site; otherwise, it is an expansion site. A site selection model is consequently constructed based on multiple construction influencing factors:

$$max \sum_i^N X_i h_i F_i \tag{17}$$

$$\sum_i X_i = N \qquad \forall i \in M \tag{18}$$

$$X_i + X_j \le l_{ij} + 1 \quad \forall i, j \in M \tag{19}$$

$$X_i + X_j \leq k_{ij} + 1 \quad \forall i \in M, k \in S \tag{20}$$

$$l_{ij} = \begin{cases} 1 & if \;\; d_{min} \leq \sqrt{\left(d_i^x - d_j^x\right)^2 + \left(d_i^y - d_j^y\right)^2} \leq d_{max} \\ 0 & else \end{cases} \tag{21}$$

$$k_{ij} = \begin{cases} 1 & if \;\; d_{min} \leq \sqrt{\left(d_i^x - s_k^x\right)^2 + \left(d_i^y - s_k^y\right)^2} \leq d_{max} \\ 0 & else \end{cases} \tag{22}$$

where N is the total number of preset expansion sites; h_i is the combined heat value of the POI of site i; F_i is the integrated index of site i. l_{ij} and k_{ij} are 0–1 distance constraint variables; d_{min} is the minimum distance constraint, set as 600 m; d_{max} is the maximum distance constraint, set as 2000 m.

The objective function (17) represents the maximization of the combined heat value of the POIs of the expansion site and the integrated index of the factors affecting construction; constraint (18) indicates that the total number of selected expansion sites is unique and fixed; constraints (19) and (20) require distance constraints between any two alternative sites, and between any alternative site and the planned site.

Parameters for the site selection model are initialized. From the initial set of 2286 points after screening, denoted as candidate site set M, longitude and latitude coordinates are extracted using ArcGIS for both M and the existing site set S. With a preset total of 20 sites N, the simulated annealing algorithm is applied to solve the model. Each of the four plans undergoes 100 simulation runs, with the top three results based on the highest objective function values selected as final outcomes. The results are presented in Table 2.

Table 2. Results of site selection model solution.

Program Type	Extension Site Number	Objective Function Value
Economic optimal	(147, 352, 527, 561, 589, 609, 709, 1354, 1503, 1612, 1670, 1886, 1894, 1900, 2008, 2062, 2111, 2117, 2137, 2261)	−8419.20
	(9, 266, 486, 610, 827, 997, 1044, 1139, 1231, 1605, 1675, 1699, 1738, 1797, 1815, 1949, 2003, 2067, 2227, 2237)	−8456.60
	(44, 99, 105, 225, 256, 401, 460, 482, 504, 572, 893, 904, 951, 1356, 1447, 1777, 1790, 1861, 1930, 1964)	−8765.27
	(70, 87, 93, 131, 139, 320, 434, 531, 672, 913, 1183, 1368, 1429, 1545, 1688, 1759, 1777, 1829, 2068, 2112)	−8256.27
	(25, 44, 291, 350, 367, 698, 702, 742, 849, 1071, 1328, 1358, 1561, 1834, 1876, 1884, 1911, 1970, 2015, 2057)	−8791.15
Environment optimal	(196, 540, 554, 562, 590, 623, 655, 754, 844, 860, 1358, 1429, 1594, 1705, 1821, 1835, 1855, 1929, 2087, 2204)	−8599.14
	(186, 266, 289, 350, 426, 594, 1156, 1176, 1234, 1382, 1548, 1591, 1663, 1685, 1722, 1750, 1971, 1981, 2195, 2202)	−8604.96
	(38, 84, 107, 123, 221, 299, 383, 466, 561, 605, 952, 1151, 1280, 1874, 1894, 1904, 1918, 1986, 2151, 2212)	−7643.59
	(50, 145, 150, 227, 305, 485, 511, 620, 651, 1031, 1053, 1080, 1156, 1165, 1191, 1351, 1679, 1752, 1894, 2021)	−8771.56
	(285, 301, 374, 582, 740, 823, 896, 928, 997, 1678, 1791, 1812, 1821, 1880, 1899, 1976, 2072, 2076, 2150, 2245)	−8163.35

Table 2. *Cont.*

Program Type	Extension Site Number	Objective Function Value
Transport optimal	(57, 115, 134, 190, 277, 536, 838, 884, 981, 1073, 1099, 1197, 1251, 1499, 1575, 1737, 1846, 1974, 1986, 2078)	10,500.08
	(61, 139, 316, 406, 481, 694, 792, 830, 836, 924, 1142, 1258, 1275, 1419, 1458, 1473, 1594, 1606, 1614, 1773)	11,065.33
	(207, 343, 358, 365, 454, 506, 1014, 1197, 1198, 1206, 1255, 1304, 1358, 1422, 1476, 1483, 1765, 1972, 2149, 2156)	10,304.90
	(274, 513, 611, 776, 900, 943, 957, 1007, 1048, 1115, 1169, 1267, 1354, 1386, 1500, 1557, 1654, 1815, 1875, 2243)	10,373.07
	(21, 68, 366, 447, 628, 718, 794, 960, 1033, 1050, 1139, 1146, 1369, 1377, 1411, 1433, 1508, 1566, 1875, 2235)	10,703.63
Integrated optimal	(91, 157, 224, 228, 257, 693, 759, 890, 1169, 1190, 1262, 1271, 1325, 1832, 1873, 1889, 1910, 1984, 2171, 2265)	−3355.31
	(78, 305, 338, 446, 521, 638, 657, 832, 1151, 1199, 1557, 1593, 1838, 1973, 2082, 2122, 2131, 2144, 2208, 2260)	−3128.45
	(39, 47, 180, 216, 659, 681, 726, 929, 932, 994, 1556, 1617, 1663, 1735, 1736, 1766, 1859, 2127, 2161, 2231)	−3340.56
	(13, 33, 242, 258, 478, 794, 869, 935, 956, 987, 1139, 1271, 1377, 1512, 1708, 1736, 1772, 1830, 1866, 2190)	−3240.26
	(0, 105, 196, 257, 374, 445, 573, 650, 795, 874, 1034, 1288, 1424, 1691, 1692, 1871, 1944, 2018, 2164, 2249)	−3080.89

3.1.2. Rail Transit Network Expansion Plan

The model results are imported into ArcGIS, where point features based on different expansion plans are extracted into separate layers. Due to the constraints only being ensured within each operation's results, sites failing distance constraints across the five operations are aggregated in ArcGIS to determine the final expansion site. Based on site distribution and integrated accessibility analysis, expansion plan lines are drawn for each expansion plan. Visualizations of these plans are shown in Figure 7.

3.2. Evaluation of Solutions Based on Accessibility

Network datasets were derived from data for the four expansion plans, analyzed using the POI-based weighted average travel time model.

The maximum values of comprehensive travel costs of initial state, economic optimal, environment optimal, transport optimal, and integrated optimal are calculated as 205.6224, 135.7255, 135.7258, 135.7254, and 135.7125, respectively. All correspond to Houzhenzi Town TAZ. According to the analysis of the average maximum travel cost of the four expansion plans and the maximum travel cost of the initial state, the zone with the longest travel cost time (i.e., Houzhenzi Town) within the Xi'an metropolitan area has been shortened by an average of 34%, which shows that the four expansion plans have significantly improved the comprehensive accessibility of the TAZ. Meanwhile, the average values are calculated as 66.4151, 58.8353, 58.8372, 58.8162, and 58.8079, respectively. Compared with the initial state, the comprehensive travel cost of each expansion plan decreased by an average of 11.4%. Kruskal–Wallis test [44] is used to access whether significant differences exist in comprehensive transportation accessibility among the four expansion plans. The calculation formulas of KW test statistic H for multi-sample differences are as follows [45]:

$$S_{SSt} = \sum_{j=1}^{k} n_j \left(\overline{R_j} - \overline{R}\right)^2 \tag{23}$$

$$S_{MST} = \frac{n(n+1)}{12} \tag{24}$$

$$H = \frac{S_{SSt}}{S_{MST}} = \frac{\sum_{j=1}^{k} n_j \left(\overline{R_j} - \overline{R}\right)^2}{n(n+1)/12} \tag{25}$$

where $\overline{R_j}$ is the rank average of the j-th sample; $\overline{R}$ is the rank average of the total samples; S_{SSt} is the sum of squares between samples; S_{MST} is the total mean square; k is the number of sample groups; n_j is the j-th sample size, $n_j = 330$, $j = 1, 2, 3, 4$; n is the total sample size.

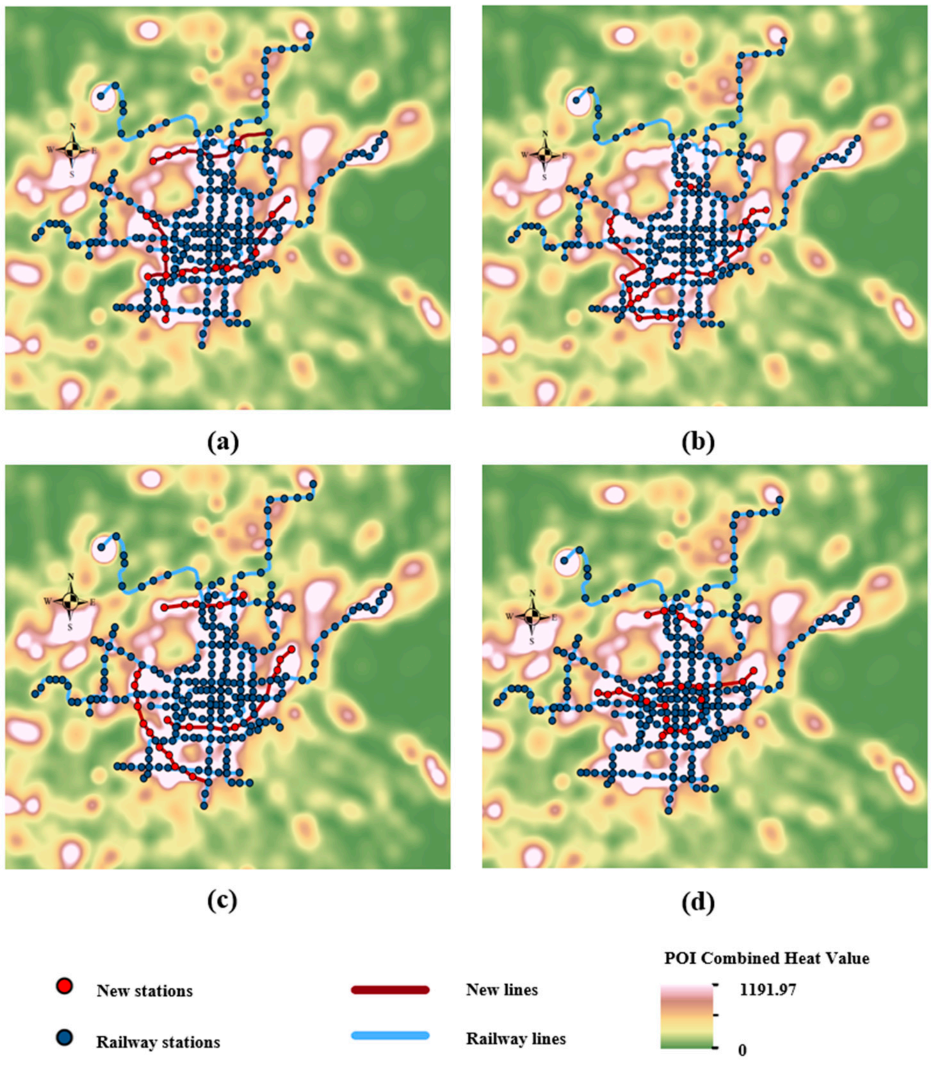

Figure 7. Expansion plans: (**a**–**d**) are, respectively, economic optimal plan, environment optimal plan, transport optimal plan, and integrated optimal plan.

According to the H value, the corresponding significant p value can be calculated. When $p < \alpha$ (α is the significance level; $\alpha = 0.05$), it means that there is a significant difference between the samples. The results show that the H value is 0.0373 and the p value is 0.9981 (>0.05); the differences among the plans are not significant. The reason is analyzed as follows: although there are significant differences in station selection and line direction among the four expansion plans, they are all located in the subway system expansion plan. At the metropolitan area scale, the travel cost differences among the four expansion plans are not significant. Therefore, it is necessary to further compare and evaluate the four plans in combination with other factors.

4. Plan Evaluation Based on Multi-Level Rail Transit Network Resilience

4.1. Quantification of Resilience Index Based on Resilience Curve

Common measurement indicators on rail transit network resilience include the proportion of remaining nodes and network efficiency. The proportion of remaining nodes can accurately reflect the changes in node status in the network, but ignores the consideration of network connectivity, resulting in isolated nodes after the failed nodes are deleted. As a commonly used measurement indicator in complex networks, network efficiency generally reflects the changes in network connectivity and the effectiveness of the network, which, however, have two fatal problems:

- If the network update strategy of retaining the largest connected subgraph is not adopted, a large number of nodes will be disconnected after the failed nodes are deleted, and the shortest travel time becomes infinite, resulting in the network efficiency being almost 0.
- If the network update strategy of retaining the largest connected subgraph is adopted, the overall scale of the network will decrease as the failed nodes are deleted, and the network efficiency will increase instead.

Therefore, the maximum connected subgraph ratio (MCSR) is used as a network performance measurement indicator, which can reflect the changes of connectivity in the network. By retaining the maximum connected subgraph at each fault transmission, the impact of the transmission fault can be cut off in time and focus on the impact of faults caused by passenger overload. The functional curve method [46,47] is employed to construct the maximum connected subgraph ratio (MCSR) curve, which serves as an indicator for assessing the resilience of multi-level rail transit networks. The relevant indicators include redundancy, recoverability, robustness, resourcefulness, adaptability, resilience loss, and resilience. The quantitative description is shown in Equations (26)–(32), with the MSCR curve shown in Figure 8, and the corresponding definition of the parameters are provided in Table 3:

$$R_1 = 1 - \left| \frac{C_1}{C_0} - 1 \right| / (t_b - t_0) \tag{26}$$

$$R_2 = \left| \frac{C_2}{C_0} - \frac{C_1}{C_0} \right| / (t_d - t_{\mathrm{b}}) \tag{27}$$

$$R_3 = C_1 / C_0 \tag{28}$$

$$R_4 = 1 - (t_d - t_0)/\mathrm{T} \tag{29}$$

$$R_5 = C_2 / C_0 \tag{30}$$

$$\Delta S = \sum_{i=t_0}^{t_d} \left(1 - \frac{C_{t_i}}{C_0}\right) \tag{31}$$

$$R_{total} = \frac{C_0 t_0 + C_0[(t_d - t_0) - \Delta S] + C_2(T - t_d)}{C_0 t_0 + C_0(t_d - t_0) + C_0(T - t_d)} \tag{32}$$

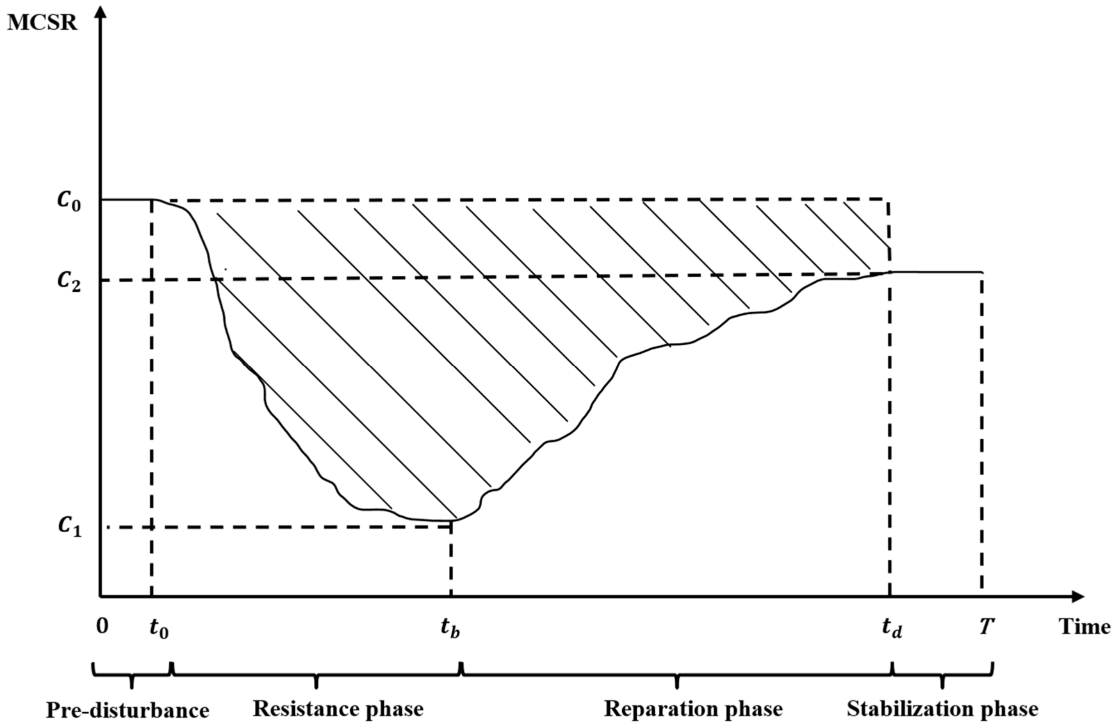

Figure 8. Rail transit network resilience curve.

Table 3. Rail transit system resilience index parameters and meanings.

Parameter	Definition
R_1 (Redundancy)	Network's initial stage resilience resist risks, indicated by the absolute slope of the resistance phase in Figure 8.
R_2 (Recoverability)	Network's ability to recover to normal operation, indicated by the slope of the reparation phase in Figure 8.
R_3 (Robustness)	Network's maximum ability to resist disturbances, defined as the ratio of the minimum MCSR value to C_0.
R_4 (Resourcefulness)	Network's ability to maintain normal operation during disturbances, defined as the ratio of normal operation time to the full cycle time.
R_5 (Adaptability)	Network's reparation effect after disturbances, defined as the ratio of the MCSR of the sta-bilization phase to C_0.
ΔS (Resilience loss)	The shaded area in Figure 8.
R_{total} (Resilience)	The area between the resilience curve and the coordinate axis in Figure 8.
i	Time intervals, measured in minutes.
C_0	MCSR of initial network, defined as 1.
C_1	Minimum value of MCSR of the network during the full cycle time.
C_2	MCSR of the network at stabilization phase.
C_{t_i}	MCSR of the corresponding network at any moment t_i.
t_0	Moments corresponding to the occurrence of disturbances.
t_b	Moments corresponding to the lowest network efficiency.
t_d	Moment when the network is restored to the new service state.
T	Disturbance full cycle time.

4.2. Failure–Reparation Model

4.2.1. CML Cascading Failure Model Based on Passenger Flow Weighting

The cascading failures in the rail transit network were explored, where the damage to a line or station triggers collapses due to passenger flow exceeding capacity, affecting other stations or lines. Existing studies mainly employ two types of methods for modeling cascading failures: the load-capacity model and the coupled map lattice (CML) model. In this study, the CML model is chosen to incorporate passenger flow redistribution and consider station backup resources [48] during the cascading failure process. The classic CML model, initially proposed by Kaneko [49] for system dynamics studies, is formulated as a one-dimensional model, as shown in Equation (33):

$$x_{t+1}(i) = \left| (1-\delta) f(x_t(i)) + \frac{\delta \sum_{\substack{j=1 \\ j \neq i}}^{N} a_{ij} f(x_t(j))}{k(i)} \right| + R \tag{33}$$

where $x_{t+1}(i)$ is the state value of node i in time period t+1; δ is the coupling index between nodes, used to describe the degree of mutual influence between nodes, with the value generally in (0, 1); a_{ij} is a 0–1 variable, used to indicate whether there is a direct edge connecting node i and node j. If there is an edge, a_{ij} =1, otherwise it is 0; $k(i)$ is the degree of node i; $f(x)$ is the mapping function, and $f(x) = 4x(1-x)$ is generally used [50]; R is the applied disturbance.

The classic CML model typically imposes a random disturbance (R) based solely on network structure, neglecting network flow influence, while the passenger flow disturbance is incorporated in this study. The redistributed passenger flow to other nodes following a node failure is considered as the disturbance (R). Equation (34) outlines the calculation of R.

$$R = Q_t'(i)/C_i \tag{34}$$

where $Q_t'(i)$ is the passenger flow added to node i after passenger flow redistribution in period t; C_i is the maximum capacity of node i.

This study evaluates the resilience of the four expansion plans, in which a random attack is designed to simulate natural disasters by initiating failure with a randomly generated node sequence. The method deletes failed nodes and the directly connected edges, redistributes passenger flow load across the network, and updates node statuses accordingly. Nodes exceeding maximum capacity post-redistribution are marked as failed. Here, t represents one minute in real time during the failure process.

4.2.2. Optimal Reparation Timing Model under Resource Constraints

Repairing all failure nodes simultaneously requires substantial manpower, materials, and financial resources, which is generally impossible. Thus, effectively managing repairs under resource constraints is crucial. Proposing an optimal repair timing model based on resource constraints, the optimal nodes repair order is obtained by solving the model, with the assumptions as follows:

- The reparation process starts immediately after the interference ends.
- Only one reparation team, that is, in each time interval, only one node is repaired in the entire network.
- Node reparation time is related to the node degree, which is set as the node degree value (k) $\times$ time interval (t), where the time interval t is the same as in the failure model and defined as the real time 1 min.

Suppose the set of reparation periods is $Y = \{1, 2, \ldots, i, \ldots, y\}$, $i = 1, 2, \ldots, y$; the set of failed nodes is $B = \{1, 2, \ldots, j, \ldots, n\}$, $j = 1, 2, \ldots, b$. A 0–1 decision variable x_{ij} is introduced to indicate whether the failed node j is scheduled to repair during the i-th reparation period;

1 means reparation, otherwise no reparation. The optimal reparation sequence is modeled under resource constraints as follows [48]:

$$maxR_r = \max\sum_{i=1}^{y} \frac{[C_i - C_{i-1}]}{T_i} \tag{35}$$

$$x_{ij} \in \{0,1\} \tag{36}$$

$$\sum_{i=1} x_{ij} \leq 1, \quad \forall j \in B \tag{37}$$

$$\sum_{j=1} x_{ij} \leq 1, \quad \forall i \in Y \tag{38}$$

$$t_c < t_i \leq t_d, \quad \forall i \in Y \tag{39}$$

$$T_i = K_i, \qquad \forall i \in Y \tag{40}$$

$$t_d = \sum_{i=1}^{y} T_i + t_c \tag{41}$$

where R_r represents the network reparation capability; i is the reparation period number; C_i represents the MCSR of the i-th reparation period; T_i represents the time spent in the i-th reparation period, that is, the number of time intervals t contained in the i-th reparation period; t_c is the start time of the reparation process; t_i is the corresponding period of the i-th reparation; t_d is the corresponding end time of the reparation process.

The objective function (35) maximizes the reparation capability of the multi-level rail transit network, focusing on the average increase in MCSR proportion during reparation periods. Constraints (37) and (38) restrict the reparation resources, allowing only one failed node to be repaired per period. Constraint (39) imposes time restrictions, ensuring that each reparation period fits within the total reparation process duration.

4.3. Program Evaluation from a Resilience Perspective

4.3.1. Passenger Flow Data Processing

This study focuses on the multi-level rail transit network of the metropolitan area, encompassing metro, suburban rails, intercity rails, and high-speed rails. Passenger flow data from 5 June 2023 are utilized, with necessary predictions for expanded or new added stations, including forecasting based on network structure and regional attributes as below.

(i) Metro station passenger flow prediction

The degree and betweenness centrality values of the station are used as network structure attributes; the regional attributes mainly include the development status, passenger flow potential, and potential attraction of the area where the station is located, selecting GDP, population, and number of scenic spots as the indicators.

(ii) Passenger flow prediction for high-speed rail, intercity, and urban rail stations

As some high-speed rails stop at few stations within the metropolitan area, global network metrics, e.g., betweenness centrality, become less relevant, favoring indicators that reflect relative node relationships. Thus, station-level attributes such as line type (defined as 3 for high-speed rail, 2 for intercity, and 1 for urban rail) and proximity centrality are chosen. Proximity centrality, as calculated in Equations (42) and (43), measures station importance relative to the connections. Regional attributes such as economic and population data of the station area also require these metrics.

$$d_i = \frac{1}{N-1}\sum_{j=1}^{N} d_{ij} \tag{42}$$

$$CC_i = 1/d_i \tag{43}$$

where d_{ij} is the shortest path between node i and node j; d_i is the average distance from node i to the remaining nodes; CC_i is the closeness centrality of node i.

The prediction method employs a multi-layer perceptron model (MLP), with data split into training (80%) and validation (20%) sets. To mitigate overfitting, L2 regularization and early stopping criteria are applied. The early stopping patience parameter is set to 5; the training procedure halts if validation set loss does not improve over five consecutive iterations. The optimal MLP model achieves a training loss of 0.0099 and a validation loss of 0.0256, in which performance metrics include MAE of 0.0628 and RMSE of 0.0732.

4.3.2. Network Data Processing

NetworkX [51] in Python3.11 is utilized to integrate four rail transit networks via transfer stations, and the Space-L method is applied to construct a multi-level rail transit network for the Xi'an metropolitan area. The merged network consists of 299 nodes and 324 edges, with a diameter of 41 and a global efficiency of 0.1023. Figure 9 visualizes the network, using warm and cold colors to depict node degree values.

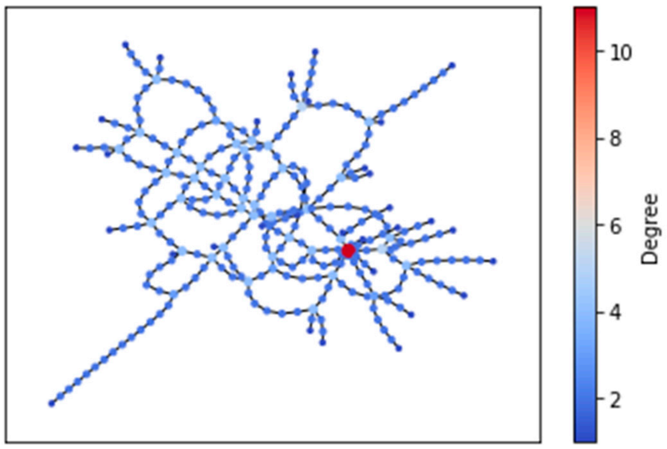

Figure 9. Network topology of multi-level rail transit system in Xi'an metropolitan area.

4.3.3. Resilience Assessment

Using passenger flow data, the Space-L method is introduced to construct a passenger flow-weighted multi-level rail transit network, incorporating newly added stations and lines from each expansion plan. The resulting network for all four plans consists of 319 nodes, with edge counts as follows: economic optimal (360), environment optimal (363), transport optimal (361), and integrated optimal (362).

The operating time periods from 6:00 to 24:00 are numbered from 1 to 18. The time-divided passenger flow of each line is visualized in Figure 10. An interesting phenomenon is that the passenger flow of the subway and the new plan lines has obvious morning and evening peak characteristics, concentrated in time period 3 (8:00–9:00) and time period 14 (19:00–20:00). The passenger flow of urban rail and intercity rail lines only has obvious morning peak characteristics, while the high-speed rail passenger flow is in time periods numbered 4–14 (9:00–20:00). Further analyses show that the possible reasons are that the subway, new planned lines, urban railways, and intercity railways are mainly used for commuting within the urban area, especially the early morning commuting; while due to the departure schedule of the high-speed rail lines, most trains are operated between 9:00 and 20:00. As passengers need a certain commuting time to go to the high-speed rail station or leave the high-speed rail station for their destinations, the high-speed rail line operation and management department needs to take this commuting time into consideration when designing the train timetable.

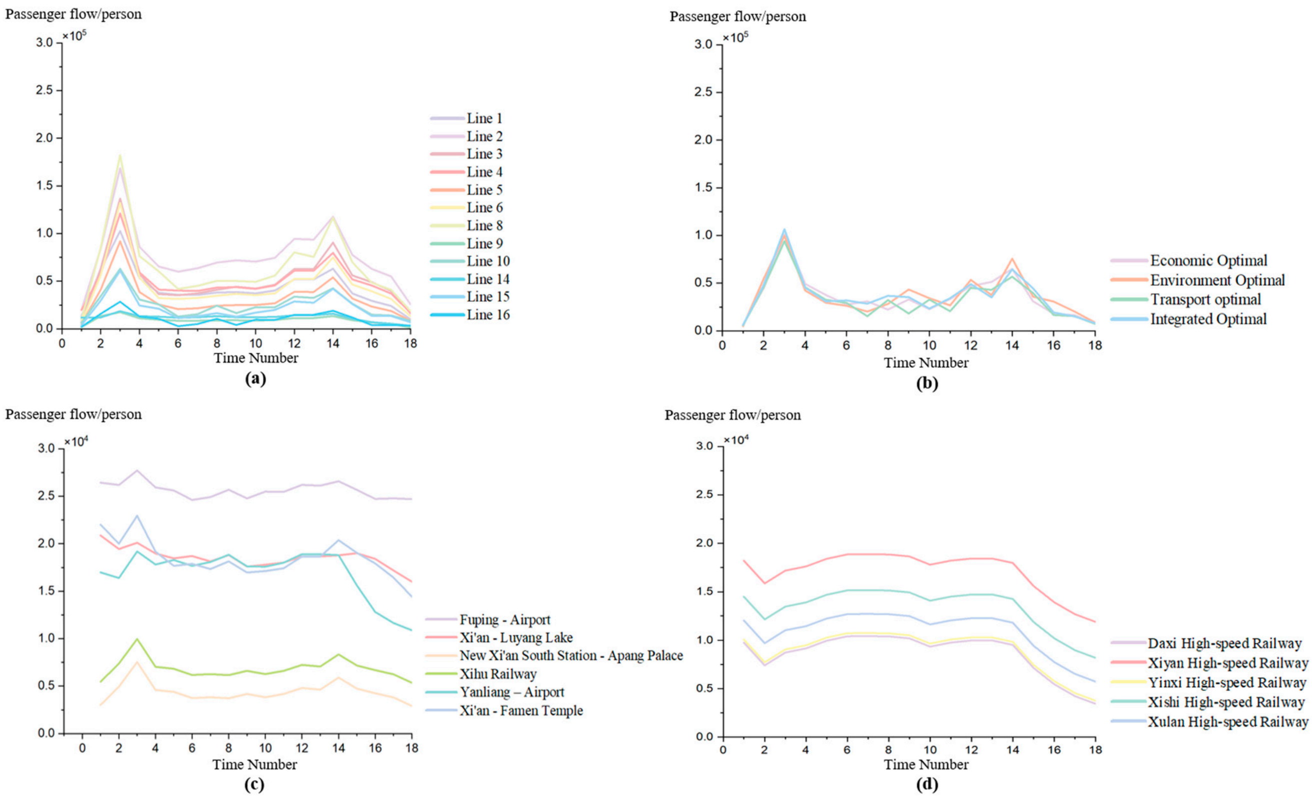

Figure 10. Passenger flow by route; (**a**–**d**) represent metro, four expansion plans, urban and intercity railways, and high-speed railway, respectively.

According to Figure 10, the difference between the peak period (8:00–9:00) and the off-peak period (15:00–16:00) attacks were analyzed. We selected one of the same station as the initial fault node in each of the two periods, set the initial fault time to the second minute, and updated the MCSR every 4 min. The results show that the rail network reached a new stable stage at the 48th minute during the peak period, when the MCRS was 0.0468, while the off-peak period reached a new stable state at the 12th minute, when the MCRS was 0.9599. During the peak passenger flow period, the damage to the entire multi-level rail transit network caused by the damage to the station was much greater than during the off-peak period.

To assess the network resilience of the four plans, two sets of experiments were designed for further analyses: (1) Time period 3 (8:00–9:00) was selected as the peak passenger flow scenario for network robustness analysis; (2) the entire operating period was selected for "failure–reparation" simulation analysis.

(1) Peak passenger flow scenario:

In this scenario, the top ten stations in terms of passenger flow are shown in Table 4.

Table 4. Station name and passenger flow.

Name	Passenger Flow (Unit: Person)
Zhangba 1st Road	14,008
Keji Road	11,566
Yanpingmen	11,260
Longshouyuan	10,786
Municipal Library	9979
Yuhuazhai	9229
Weiqunan	8943
Xiaozhai	8863

Using a random attack method, a station is randomly selected from the top ten stations in passenger flow as the initial failure node. The simulation results are shown in Figure 11, in which the new stable state enclosed by the red rectangle. The network is updated every 4 min, and the simulation time period is extended to 72 min to better observe the new stable state after failure.

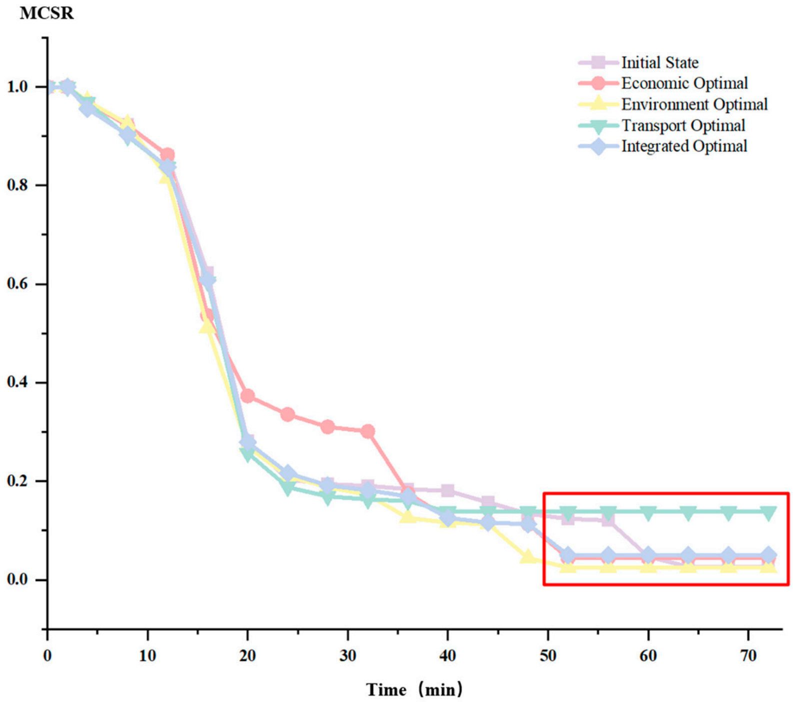

Figure 11. Failure simulation in the morning rush hour scenario.

After attaining the stable stage in Figure 11, the MCSR of initial state, economic optimal, environment optimal, transport optimal, and integrated optimal are 0.0268, 0.0439, 0.0251, 0.1379, and 0.0502. Since MCSR shows a downward trend over time and does not conform to the normal distribution, variance analysis is not suitable for analyzing the differences between various plans and initial state networks after the steady state. Therefore, this study uses the KW test to analyze the difference in continuous steady state. The analysis results are as follows: H value is 14 and p value is 0.0073 (<0.05), that is, there are significant differences between the steady state results in the statistical analysis. Combined with Equation (28), the robustness of the transport optimal expansion plan is 0.1379, which is 4.14 times higher than the initial network. According to the maximum connected subgraph ratio (MCSR) after reaching the new stable state and the number of nodes in the network (299 in the initial state and 319 in the four expansion plans), the transport optimal expansion plan still retains 44 nodes in the remaining maximum connected subgraph, while the initial state network has only 8 nodes remaining.

(2) Entire operating period simulation:

In this scenario, the "failure–reparation" model is used to simulate the four expansion plans, respectively, and the initial failure sequence is randomly generated: {Xiaozhai, Daming Palace West, Xi'an North Station, Afang Palace, Fuping-Yanliang, Poyang North, Jinghe, Jingyang, Louguan, Sanyuan}, a total of 10 nodes. The first 6 min are set as normal operation as the warm-up time. The failure simulation starts from the 6th minute. Based on the elasticity curve, the elasticity indicators of the multi-level rail transit network under each plan are analyzed, as shown in Figure 12. The right side shows the whole failure–reparation simulation process of the four plans, and the local enlarged figure on the left side shows the MCSR curve of each plan from the start (0 minute) to the end of the failure stage.

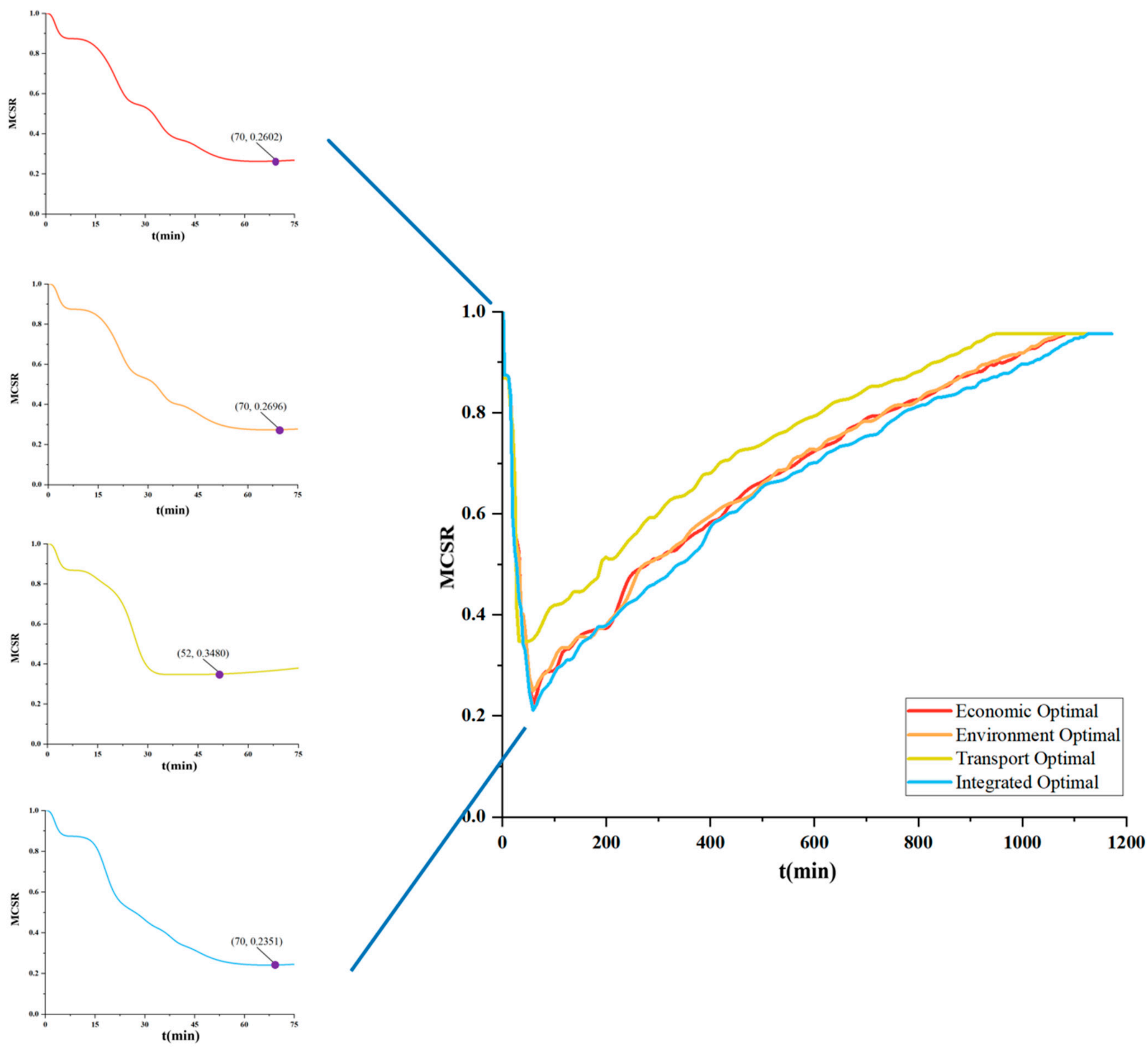

Figure 12. MCSR curves from failure–reparation simulation for the four expansion plans.

According to the resilience curves in Figure 12, the resilience indicators of each plan are calculated, with the values shown in Table 5.

Table 5. Comparison of resilience indicators of the four expansion plans.

Quantitative Indicator	Economic Optimal	Environment Optimal	Transport Optimal	Integrated Optimal
Disturbance start time t_0 (min)	6	6	6	6
Disturbance end time t_b (min)	70	70	52	70
Disturbance duration (min)	[6, 70]	[6, 70]	[6, 52]	[6, 70]
Minimum MCSR	0.26	0.27	0.348	0.235
Repair start time t_b (min)	70	70	52	70
Repair end time t_d (min)	1084	1076	950	1172
Repair duration (min)	[70, 1084]	[70, 1076]	[52, 950]	[70, 1172]

Table 5. *Cont.*

Quantitative Indicator	Economic Optimal	Environment Optimal	Transport Optimal	Integrated Optimal
MCSR after restoration	0.956	0.956	0.956	0.956
Redundancy (R_1)	0.9884	0.9886	0.9858	0.9880
Recoverability (R_2)	6.863×10^{-4}	6.824×10^{-4}	6.772×10^{-4}	6.543×10^{-4}
Robustness (R_3)	0.26	0.27	0.348	0.235
Resourcefulness (R_4)	0.0055	0.0093	0.1259	0.0051
Adaptability (R_5)	0.956	0.956	0.956	0.956
Resilience loss (ΔS)	421.01	414.4	372.69	470.13
Resilience (R_{total})	0.612	0.616	0.65	0.603

Based on Figure 12 and Table 5, the following conclusions are drawn:

(1) Robustness analysis: The minimum MCSR of the four plans when they reach a stable state after damage is 0.26, 0.27, 0.348, and 0.235. The KW test analysis shows that the H value is 11.0 and the p value is 0.012 (<0.05). There is a significant difference, among which transport optimal has the highest robustness (0.348), which is 1.48 times the lowest robustness integrated optimal (0.235).

(2) Recoverability analysis: The recoverability of the four expansion plans is very low. This is because, according to the definition of Equation (27), the slope of the repair stage is used to represent the restoration. The MCSR value range is 0–1, the horizontal axis is the maximum value of more than 1000, and the model assumes that only one node can be in the repair state in each time t, resulting in a longer complete repair time. This indicator is low in the four plans and there is no significant difference.

(3) Resilience analysis: According to Equation (32), the resilience index ranges from 0 to 1, where the closer it is to 1, the better the network resilience. The resilience of the four plans is 0.612, 0.616, 0.65, and 0.603, among which transport optimal has the highest resilience (0.65), which is 7.2% higher than the integrated optimal plan (0.603) with the lowest resilience.

Based on the above two scenarios, the transport optimal plan has the best robustness in large passenger flow scenario and the best resilience in the entire operation cycle. Therefore, the transport optimal plan should be given priority. However, it is worth noting that in two scenarios, the changes in the minimum spanning tree (MCSR) across the four plans during both the failure process and the repair process exhibit minimal variation. The reason for this is related to the attack method and evaluation indicators used in this study. The attack method set in this study is to first redistribute the passenger flow of the failed node to its neighboring nodes, then delete the failed node and its edges, and, finally, identify the largest connected subgraph in the new network and update the network. Since there may be multiple connected subgraphs in the network after deleting the failed node, using the largest connected subgraph as the new network will cause some normal nodes in other connected subgraphs to be discarded, which also means that even if the damaged nodes are different, the network may still reach the same state after the update.

5. Conclusions

This paper proposes a rail transit expansion strategy based on multiple construction influencing factors, in which a network evaluation method was constructed from the perspectives of accessibility and resilience. By taking Xi'an metropolitan area as an empirical case study, four rail transit growth plans were designed, of which the integrated accessibility of the area was significantly improved. The resilience of the multi-level rail transit network under each plan was evaluated based on the "failure–reparation" model and the resilience curve. Finally, the growth plan with the best accessibility and resilience was determined. Both the proposed rail transit network growth plan and evaluation method have certain practical significance, particularly in solving the current insufficient accessibility problem during the metropolitan development. The plans and the evaluation methods may be applied to the development of other metropolitan areas. Specifically, data on transportation routes and stations, population and economic data, and land use type data are needed [52,53]. An expansion model based on multiple construction factors was analyzed to draw up a rail transit network expansion plan, and then the accessibility and resilience assessment method in this study was used for detailed analysis. This framework can be applied to the multi-level rail system improvement and planning of primary metropolitan areas.

Although the results are promising, this study, indeed, has limitations with regards to the rail transit growth plan and evaluation method. First, the expansion plan lacks consideration of factors such as terrain and slope in the line design part. Future studies may introduce land type and slope factors, and use the taboo search (TS) algorithm to determine the line trend based on the expansion station. Second, during the resilience evaluation, this study constructed a multi-level rail transit network based on passenger flow weighting. However, some predictions may deviate due to the limited number of rail transit stations. Future research could include time factors and expand training data with passenger flow across different periods.

Author Contributions: The authors confirm contribution to the paper as follows: Study conception and design: Y.Z. and D.S.; data collection: L.L. and Z.Z.; analysis and interpretation of results: Y.Z.; draft manuscript preparation: Y.Z., L.L., Z.Z., and D.S. All authors reviewed the results. All authors have read and agreed to the published version of the manuscript.

Funding: This research was funded in part by the National Nature Science Foundation of China [71971138, 52172319] and the National Social Science Foundation of China [22XJY030], and the APC was funded by [52172319]. Any opinions, findings and conclusions or recommendations expressed in this paper are those of the authors, and do not necessarily reflect the views of the sponsors.

Data Availability Statement: All data, models, and codes that support the findings of this study are available from the corresponding author upon reasonable request.

Conflicts of Interest: The authors declare that they have no conflicts of interest.

References

1. CEIC. Available online: https://www.ceicdata.com.cn/zh-hans/china/public-transit-summary (accessed on 20 September 2024).
2. Chen, F.; Yin, Z.; Ye, Y.; Sun, D.J. Taxi Hailing Choice Behavior and Economic Benefit Analysis of Emission Reduction Based on Multi-mode Travel Big Data. *Transp. Policy* **2020**, *97*, 73–84. [CrossRef]
3. Zhang, Y.; Zhao, M. Spatial Delineation, Characteristics Analysis, and Classification of China's Metropolitan Regions. *Urban Planning Forum.* **2023**, *2*, 67–76. (In Chinese)
4. Wan, G.; Sun, D.J.; Peng, B.; Mao, X. Risk Assessment of Urban Transportation Complex Hub from Resilience Perspective: An Empirical Study on Xi'an North Railway Station. *Nat. Hazards Rev.* **2024**, *25*, 0402404. [CrossRef]
5. Wu, S.; Sun, D.J.; Qiu, G. Emission Analysis Based on Mixed Traffic Flow and License Plate Recognition Models. *Transp. Res. Part D Transp. Environ.* **2024**, *134*, 104331. [CrossRef]
6. Nian, G.; Pan, H.; Huang, J.; Sun, D.J. Labor supply decisions of taxi drivers in megacities during COVID-19 pandemic period. *Travel Behav. Soc.* **2024**, *35*, 100745. [CrossRef]
7. Bussieck, M.R.; Winter, T.; Zimmermann, U.T. Discrete optimization in public rail transport. *Math. Program.* **1997**, *79*, 415–444. [CrossRef]
8. Li, A.; Wang, D.; Peng, Q.; Wang, L. Path-Based Approach for Expanding Rail Transit Network in a Metropolitan Area. *J. Adv. Transp.* **2022**, *2022*, 7637298. [CrossRef]
9. Ghorbanzadeh, M.; Effati, M.; Gilanifar, M.; Ozguven, E.E. Subway station site selection using GIS-based multi-criteria decision-making: A case study in a developing country. *Comput. Res. Prog. Appl. Sci. Eng.* **2020**, *6*, 60–69.
10. Cai, Z.; Wang, J.; Li, T.; Yang, B.; Su, X.; Guo, L.; Ding, Z. A novel trajectory based prediction method for urban subway design. *ISPRS Int. J. Geo-Inf.* **2022**, *11*, 126. [CrossRef]
11. Cai, J.; Li, Z.; Long, S. Integrated Optimization of Route and Frequency for Rail Transit Feeder Buses under the Influence of Shared Motorcycles. *Systems* **2024**, *12*, 263. [CrossRef]
12. Tian, F.; Liang, J.; Chen, R. Multi-Modal Urban Traffic Transfer Schedule Timetable Bi-Objective Optimization: Model, Algorithm, Comparison, and Case Study. *Transp. Res. Rec. J. Transp. Res. Board* **2024**, *2678*, 295–310. [CrossRef]

13. Lee, E.H.; Jeong, J. Assessing equity of vertical transport system installation in subway stations for mobility handicapped using data envelopment analysis. *J. Public Transp.* **2023**, *25*, 100074. [CrossRef]
14. Lee, E.H.; Shin, H.; Cho, S.H.; Kho, S.Y.; Kim, D.K. Evaluating the efficiency of transit-oriented development using network slacks-based data envelopment analysis. *Energies* **2019**, *12*, 3609. [CrossRef]
15. Kwan, M.P.; Janelle, D.G.; Goodchild, M.F. Accessibility in space and time: A theme in spatially integrated social science. *J. Geogr. Syst.* **2003**, *5*, 1. [CrossRef]
16. Meng, X.; Lin, S.; Zhu, X. The resource redistribution effect of high-speed rail stations on the economic growth of neighbouring regions: Evidence from China. *Transp. Policy* **2018**, *68*, 178–191. [CrossRef]
17. Liu, S.; Yao, E.; Li, B. Exploring urban rail transit station-level ridership growth with network expansion. *Transp. Res. Part D Transp. Environ.* **2019**, *73*, 391–402. [CrossRef]
18. Zhou, J.; Yang, Y. Transit-based accessibility and urban development: An exploratory study of Shenzhen based on big and/or open data. *Cities* **2021**, *110*, 102990. [CrossRef]
19. Li, X.; Yang, Z.; Guo, Y.; Xu, W.; Qian, X. Factoring in temporal variations of public transit-based healthcare accessibility and equity. *Int. J. Transp. Sci. Technol.* **2024**, *13*, 186–199. [CrossRef]
20. Lucas, K.; Martens, K.; Di Ciommo, F.; Dupont-Kieffer, A. (Eds.) *Measuring Transport Equity*; Elsevier: Amsterdam, The Netherlands, 2019.
21. Sun, Q. Study on the Spatial Relationship between Traffic Accessibility and Tourism Economic Linkage: Taking Daxi High-speed Railway as an Example. *Econ. Probl.* **2023**, *4*, 95–104. (In Chinese)
22. Yu, L.; Cui, M. How subway network affects transit accessibility and equity: A case study of Xi'an metropolitan area. *J. Transp. Geogr.* **2023**, *108*, 103556. [CrossRef]
23. Gao, C.; Fan, Y.; Jiang, S.; Deng, Y.; Liu, J.; Li, X. Dynamic robustness analysis of a two-layer rail transit network model. *IEEE Trans. Intell. Transp. Syst.* **2021**, *23*, 6509–6524. [CrossRef]
24. Wu, S.; Zhu, Y.; Li, N.; Wang, Y.; Wang, X.; Sun, D.J. Urban rail transit system network reliability analysis based on a coupled map lattice model. *J. Adv. Transp.* **2021**, *2021*, 5548956. [CrossRef]
25. Zhu, G.; Sun, R.; Fan, J.; Li, F.; Hou, Y.; Yu, H.; Liu, P.X. Coupling Effect and Chain Evolution of Urban Rail Transit Emergencies. *IEEE Trans. Intell. Transp. Syst.* **2023**, *25*, 1044–1053. [CrossRef]
26. Xu, X.; Huang, A.; Shalaby, A.; Feng, Q.; Chen, M.; Qi, G. Exploring cascading failure processes of interdependent multi-modal public transit networks. *Phys. A Stat. Mech. Its Appl.* **2024**, *638*, 129576. [CrossRef]
27. Hua, W.; Ong, G.P. Network survivability and recoverability in urban rail transit systems under disruption. *IET Intell. Transp. Syst.* **2017**, *11*, 641–648. [CrossRef]
28. Sun, D.J.; Guan, S. Measuring vulnerability of urban metro network from line operation perspective. *Transp. Res. Part A Policy Pr.* **2016**, *94*, 348–359. [CrossRef]
29. Yin, J.; Ren, X.; Liu, R.; Tang, T.; Su, S. Quantitative analysis for resilience-based urban rail systems: A hybrid knowledge-based and data-driven approach. *Reliab. Eng. Syst. Saf.* **2022**, *219*, 108183. [CrossRef]
30. Le, J.; Ye, K. Measuring City-Level Transit Accessibility Based on the Weight of Residential Land Area: A Case of Nanning City, China. *Land* **2022**, *11*, 1468. [CrossRef]
31. Charnes, A.; Cooper, W.W.; Rhodes, E. Measuring the efficiency of decision making units. *Eur. J. Oper. Res.* **1978**, *2*, 429–444. [CrossRef]
32. Banker, R.D.; Charnes, A.; Cooper, W.W. Some models for estimating technical and scale inefficiencies in data envelopment analysis. *Manag. Sci.* **1984**, *30*, 1078–1092. [CrossRef]
33. Shafiq, M.; Lobo, A.; Couto, A. Equity of access to rail services by complementary motorized and active modes. *J. Transp. Geogr.* **2024**, *121*, 104007. [CrossRef]
34. Shantal, M.; Othman, Z.; Bakar, A.A. A novel approach for data feature weighting using correlation coefficients and min–max normalization. *Symmetry* **2023**, *15*, 2185. [CrossRef]
35. Lee, C.; Lee, E.H. Evaluation of urban nightlife attractiveness for Millennials and Generation Z. *Cities* **2024**, *149*, 104934. [CrossRef]
36. Shaanxi Provincial People's Government. *Xi'an Metropolitan Area Development Plan*; Shaanxi Government Document No. 7: Xi'an, China, 2022. (In Chinese)
37. OpenStreetMap. Available online: https://openmaptiles.org/ (accessed on 23 November 2023).
38. AutoNavi Map. Available online: https://lbs.amap.com/ (accessed on 25 November 2023).
39. China Railway Construction Corporation Limited. Available online: http://www.fsdi.com.cn/ (accessed on 25 November 2023).
40. China Population Census Yearbook. 2020. Available online: https://www.stats.gov.cn/sj/pcsj/rkpc/7rp/zk/indexch.htm (accessed on 26 November 2023).
41. Van Beers, W.C.; Kleijnen, J.P. December. Kriging interpolation in simulation: A survey. In Proceedings of the 2004 Winter Simulation Conference, Washington, DC, USA, 5–8 December 2004; Volume 1.
42. Wu, A.; Zheng, C.; Hou, Z.; Duan, F.; Cai, Z. An Excellence Level Evaluation Model of Intelligent Manufacturing Unit. In Proceedings of the 2022 IEEE 22nd International Conference on Software Quality, Reliability, and Security Companion (QRS-C), Guangzhou, China, 5–9 December 2022; pp. 439–443.
43. Wu, S.; Li, T.; Xu, F.; Chen, R.; Zhou, X.; Wang, B. Configuration size optimization of gas-electric hybrid power systems on ships considering energy density and engine load response. *Energy Convers. Manag.* **2024**, *301*, 118069. [CrossRef]

44. Kruskal, W.H.; Wallis, W.A. Use of ranks in one-criterion variance analysis. *J. Am. Stat. Assoc.* **1952**, *47*, 583–621. [CrossRef]
45. Liu, Y.; Cao, Y.; Liu, S. Selection of State Characterization Parameters for a Low-voltage Switching Device Based on Improved Kruskal-Wallis Test. *High Volt. Eng.* **2024**, *50*, 535–542. (In Chinese)
46. Twumasi-Boakye, R.; Sobanjo, J.O. A computational approach for evaluating post-disaster transportation network resilience. *Sustain. Resilient Infrastruct.* **2021**, *6*, 235–251. [CrossRef]
47. Nian, G.; Chen, F.; Li, Z.; Zhu, Y.; Sun, D.J. Evaluating the alignment of new metro line considering network vulnerability with passenger ridership. *Transp. A Transp. Sci.* **2019**, *15*, 1402–1418. [CrossRef]
48. Cheng, J.; Lu, Q.; Wu, T.Z.; Wang, Y.Q. A Method for Evaluating Recovery Strategies for Cascade Failures of Metro Networks. *Transp. Inform. Saf.* **2023**, *41*, 173–184. (In Chinese)
49. Kaneko, K. Clustering, coding, switching, hierarchical ordering, and control in a network of chaotic elements. *Phys. D Nonlinear Phenom.* **1990**, *41*, 137–172. [CrossRef]
50. Ye, H.; Luo, X. Cascading failure analysis on Shanghai metro networks: An improved coupled map lattices model based on graph attention networks. *Int. J. Environ. Res. Public Health* **2021**, *19*, 204. [CrossRef] [PubMed]
51. Hagberg, A.; Swart, P.J.; Schult, D.A. *Exploring Network Structure, Dynamics, and Function Using NetworkX (No. LA-UR-08-05495; LA-UR-08-5495)*; LANL: Los Alamos, NM, USA, 2008.
52. Sun, D.J.; Zheng, Y.; Duan, R. Energy consumption simulation and economic benefit analysis for urban electric commercial-vehicles. *Transp. Res. Part D Transp. Environ.* **2021**, *101*, 103083. [CrossRef]
53. Sun, D.J.; Ding, X. Spatiotemporal evolution of ridesourcing markets under the new restriction policy: A case study in Shanghai. *Transp. Res. Part A Policy Pr.* **2019**, *130*, 227–239. [CrossRef]